Everyone works better together: rational improvements to radio- and immunotherapy combinations

Frijlink, E.S.

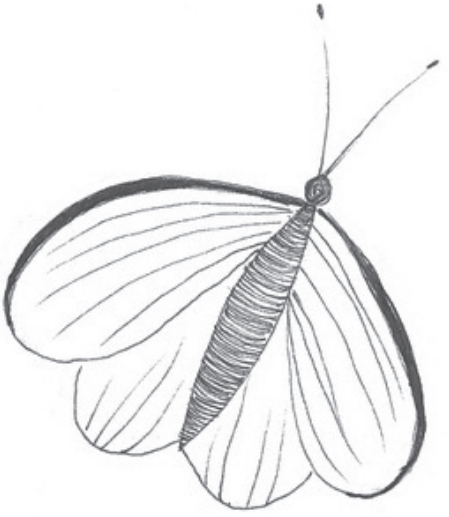

3

Identifying the mechanisms behind tumor-induced Treg priming

Elselien Frijlink[1,2], Mo D. Staal[2] and Jannie Borst[2]

[1]Division of Tumor Biology and Immunology and Oncode Institute, The Netherlands Cancer Institute, Amsterdam, The Netherlands
[2]Department of Immunology and Oncode Institute, Leiden University Medical Center, Leiden, The Netherlands.

Abstract

Tumor emergence is not only associated with local immunosuppression but also induces systemic immune disturbances. Regulatory T cells (Tregs) are among the first immune cells to respond to tumor development and may accumulate in the tumor-draining lymph node (TdLN) before migrating into the tumor. However, the mechanisms underlying tumor-induced Treg priming in the TdLN are poorly characterized. Here, using the mouse TC-1 tumor model, we demonstrate that tumor growth preferentially promotes expansion and initial differentiation in the TdLN of Helios^{+} Tregs, representative for a thymus-derived origin. These Tregs subsequently migrate into the tumor microenvironment (TME), where they adopt a more mature phenotype. We propose future experimental avenues that can reveal mechanisms dictating tumor-induced Treg responses in the TdLN and developmental trajectories of Tregs in healthy tissues and tumors. This information is essential to reveal novel therapeutic targets to inhibit Treg responses without eliciting immune-related adverse effects.

Introduction

Regulatory T cells (Tregs) are critical for maintaining immune homeostasis, but also contribute to an immunosuppressive tumor microenvironment (TME), where they inhibit the function of effector T cells and dendritic cells (DCs)[1]. Thus, Tregs may impact the prognosis of various cancer types[2] and limit the effectiveness of anti-tumor immunotherapy[3]. Consequently, targeting of Tregs may be attractive to improve therapeutic outcomes, but current approaches are challenged by 1) the shared expression of markers between Tregs and conventional T cells (Tconvs), 2) the difficulty to accurately dissect Treg and Tconv populations in human tumors[4] and 3) the need to inhibit tumor-associated Tregs, while preserving the ability of Tregs in healthy tissue to maintain tissue homeostasis[5]. Thus, gaining a deeper understanding of these cells in the tumor context may identify better therapeutic targets.

Tregs can be classified into two subsets, based on their tissue of origin: Thymus-derived Tregs (tTregs) develop from immature T cell precursors, recognize self-antigens, and act as guardians against autoimmunity, while peripherally-induced Tregs (pTregs) arise from mature Tconvs and suppress responses against non-self antigens[4]. pTregs are primarily found at mucosal-surfaces, like the colon, and the maternal-fetal interface[6,7]. tTregs generally circulate between the blood and lymphoid tissue, where they receive signals required to differentiate into effector (e)Tregs. Subsequently, these eTregs migrate into non-lymphoid tissue (NLT) to become tissue-resident Tregs[8]. Within these NLTs, Tregs functionally adapt their differentiation states in response to local $CD4^+$ Tconv cells, which produce lineage-specific cytokines associated with T helper (Th)1, Th2, or Th17 cells. In response, Tregs tailor their suppression against the corresponding Tconv population[9].

In autoimmunity treatment, anti-inflammatory tTregs are preferred due to their stable lineage commitment, while pTregs may revert back into Tconvs that can be pro-inflammatory[10]. The precise contributions of these Treg subtypes in cancer remains uncertain, due to the lack of phenotypical and functional markers to distinguish between tTregs and pTregs in human studies, until recently[11]. Accurate identification of these cells holds promise for developing novel therapeutic approaches. For instance, lineage instability in intra-tumoral Tregs can cause genetic reprogramming[12] and conversion to Tconv cells, evoking anti-tumor immune responses[13]. However, characterization of the T cell receptor (TCR) profiles of human tumor-resident Tregs identified a significant overlap with circulating Tregs isolated from blood, while no parallels were found with Tconvs[14]. This finding emphasizes that tumor-resident Tregs likely emerge not from the conversion of Tconvs but rather represent tTregs that are attracted to the TME from the circulation. Insights from single-cell RNA sequencing (scRNAseq) in mice further suggest that tumor-derived Tregs follow adaptation trajectories similar to those observed in NLTs[15], consistent with findings in human breast cancer[16]. These Tregs appear to be primed for activation in the (tumor) draining lymph node (TdLN)[15]. Thus, tumor-derived Tregs likely are derived from the circulation and show high similarities to tissue-resident Tregs in healthy neighboring tissue. Furthermore, the presence of tumors correlated with elevated levels of Tregs systemically, particularly in the TdLN[17-19]. These

Tregs can hinder the initiation of new T cell responses[20,21]. Although the role of these Tregs in driving metastases is becoming increasingly clear[18,19], the exact mechanisms of initial Treg priming in the tumor context remains controversial. Since the TdLNs serve as the site for priming and maintaining tumor-specific Tconv and Treg responses[22-24], unraveling the mechanisms that initiate and sustain Treg responses in the tumor setting is of great importance.

We have previously identified that the transplantable C57BL/6-derived lung carcinoma TC-1 tumor model[25] resembles human "lymphocyte depleted" cancer[26,27- under revision], which is discerned by lymphocyte paucity and high myeloid cell infiltrate. TC-1 tumor growth raised a spontaneous immunosuppressive response in the TdLN, characterized by increased Ly6C$^+$ monocytes and effector Tregs[27- under revision]. Thus, this tumor model allows us to monitor how tumor growth orchestrates immunosuppressive responses beyond the local TME and assess the contribution of TC-1 tumor development to Treg priming in the TdLN, spleen, and tumor. We next integrate our findings and highlight the potential future experiments required to expand upon the current understanding of tumor-induced Treg priming and their differentiation trajectories within healthy and tumor tissue.

Results

Tumor development induces Helios$^+$ Treg priming in the tumor draining lymph node

To investigate how TC-1 tumor growth impacts systemic Treg responses, we assessed the abundance of Tregs by flow cytometric analysis in the tumor, TdLN, non-TdLN, and spleen, and compared them to age-matched naïve mice. We observed that Tregs comprise the largest population of CD3$^+$ cells in the tumor (Figure **1A**). Interestingly, the frequency (Figure **1B**) and absolute number (Figure **1C**) of Tregs was significantly increased in the axillary TdLN and spleen, but not in the non-TdLN of TC-1 tumor-bearing mice. This data suggests that the TdLN serves as the priming site for tumor-induced Treg expansion, from where Tregs can disseminate systemically. To better visualize this, TC-1 tumor bearing mice received the S1P-receptor agonist FTY720, which restrains T-cell egress from lymphoid organs[28]. At day 9 post treatment, presence of FTY720 significantly enhanced the proportion of Tregs in the TdLN compared to the control group (Figure **1D**). Furthermore, FTY720 treatment significantly reduced the fraction of Tregs present in the tumor, indicating that tumor-infiltrating Tregs originate from the TdLN. These findings were further supported by the increased fraction of proliferating (Ki67$^+$) Tregs in the TdLN, while Tregs in the non-TdLN and spleen did not show enhanced proliferation compared to the naïve control group (Figure **1E**). Interestingly, analysis of the Treg population across all tissues revealed that regardless of tumor presence, the proliferating Treg subset was primarily characterized by Helios expression (Figure **1F**), a marker for tTregs in mice[29]. Quantitative analysis demonstrated that while both Helios$^+$ and Helios$^-$ Tregs exhibited increased proliferation in the TdLN of tumor-bearing mice, the majority of the proliferating Tregs expressed Helios (Figure **1G**). Furthermore,

upon TC-1 tumor growth, both Helios$^+$ and Helios$^-$ Tregs showed a significant increase in absolute numbers within the TdLN, but Helios$^+$ Tregs constituted the largest Treg population in the TdLN (Figure **1H**). Importantly, the majority of tumor-infiltrating Tregs expressed Helios (Figure **1I**). Together with the Treg depletion from the tumor upon FTY720 treatment, these data argue that Helios$^+$ Tregs expand in the TdLN and subsequently migrate into the tumor.

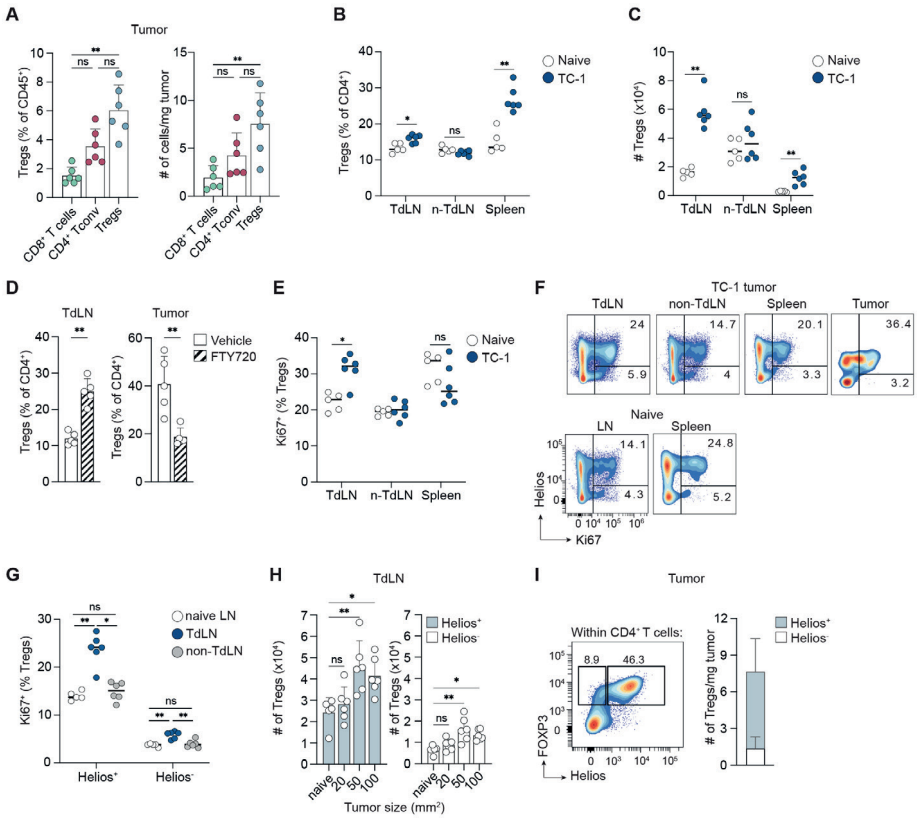

Figure 1. TC-1 tumor development drives priming of Helios$^+$ Tregs in the TdLN
Analysis of the CD3$^+$ T cell population found in the tumor, TdLN (right axillary LN), non-TdLN (left inguinal LN) and spleen of mice bearing 50 mm^2 TC-1 tumors (n=6) and age-matched naïve mice (n=5) by flow cytometry. (**A**) Frequency among CD45$^+$ cells (left) and absolute number (right) of the indicated populations found in tumor. (**B,C**) Frequency (**B**) and absolute number (**C**) of Tregs in indicated tissues. (**D**) Mice bearing TC-1 tumors (n=5/group) received FTY720 or vehicle (NaCl) by oral gavage when tumor size reached 20 mm^2 (day 0), followed by days 3 and 6. Indicated is the percentage of Tregs among CD4$^+$ T cells at day 9 post treatment found in the TdLN and tumor. (**E**) Percentage of Ki67$^+$ cells among Tregs in the indicated tissues. (**F,G**) Representative concatenated (n=5 for naïve and n=6 for TC-1 tumor bearing) flow cytometry plots (**F**) and quantification (**G**) of the percentage of Ki67$^+$ cells positive for Helios$^+$ or Helios$^-$ Tregs in the indicated tissues. (**H**) The absolute number of Helios$^+$ and Helios$^-$ Tregs found in the TdLN of TC-1 tumor bearing mice (n=6/timepoint) at increasing tumor sizes compared to age-matched naïve mice (n=5). (**I**) Representative concatenated (n=6) flow cytometry plot (left) and quantification in absolute numbers (right) of the distribution of Helios$^+$ and Helios$^-$ Tregs found in the TC-1 tumor at 50 mm^2.
Data are from one experiment, representative of at least two experiments. Error bars indicate SD. *P < 0.05, **P < 0.01, Mann-Whitney test and Kruskall-Wallis test with Dunn's post hoc analysis. ns; no significance.

Following priming, thymic-derived Tregs acquire an effector phenotype in the tumor

If Tregs were primed in the TdLN and subsequently relocated to the tumor, as suggested by our data, we would expect them to acquire an effector phenotype. We indeed observed a significant increase in the proportion of cells displaying a CD44$^+$ CD62L$^-$ effector phenotype within the Helios$^+$ Treg population, in contrast to Helios$^-$ Tregs (Figure **2A,B**). Conversely, Helios$^-$ Tregs exhibited a higher fraction of cells with a CD44$^-$ CD62L$^+$ naïve phenotype. Thus, while both Helios$^+$ and Helios$^-$ Tregs expanded in the TdLN upon TC-1 tumor growth, primarily Helios$^+$ Tregs apparently underwent effector differentiation. Reduction analysis of the total Treg population revealed a distinct population in the TdLN that was absent in both naïve and non-TdLNs (Figure **2C**). This population encompassed both Helios$^+$ and Helios$^-$ Tregs, although the majority were Helios$^+$ cells (Figure **S1A**). Clustering analysis confirmed these findings and identified clusters 5, 6 and 7 to be significantly enhanced in the TdLN, but not in the naïve and non-TdLNs (Figure **2D,E**). Interestingly, although cluster 4 was not significantly enriched in the TdLN compared to naïve LNs, it is near absent in the non-TdLN. All clusters displayed high expression of ICOS, TNFR2, CTLA-4, GITR. Furthermore, cluster 5 and 7 differentiate from cluster 6 by Helios and enhanced CCR8 expression. In addition, cluster 5 exhibits elevated PD-1, CXCR6, CD39 and OX40 expression, as compared to the other clusters (Figure **2F**, **S1B**), consistent with an NLT-adapted effector phenotype[15]. This population is likely primed to migrate and eventually become tissue-resident Tregs. Cluster 7 is highly proliferative, based on the expression of Ki67, which was less pronounced in cluster 6 and not observed in clusters 4 and 5 (Figure **2F**, **S1B**), and probably reflects a precursor population of cluster 5. Thus, TC-1 tumor development drives effector differentiation of both Helios$^+$- and Helios$^-$ Tregs in the TdLN, yet expansion of Helios$^+$ Tregs seems to be preferred.

Following differentiation into effector cells, Tregs move to non-lymphoid tissues, where they undergo further phenotypical adaptations[15]. Tumor-derived Tregs apparently undergo similar adaptation trajectories[15], but may exhibit enhanced expression of chemokine receptors, such as CCR8 and CXCR6[16]. Similarly, scRNAseq analysis in mice have illustrated a transformation process of Tregs migrating from the TdLN into the TME, where they become tumor-retained Tregs. These Tregs exhibit an upregulated protein expression profile, including enhanced ICOS and CD39 expression[30]. Correspondingly, tumor-resident Helios$^+$ Tregs were enriched for the CD44$^+$ CD62L$^-$ effector phenotype (Figure **S1C**) and exhibited increased cell surface expression of ICOS, CTLA-4, GITR and CCR8 as compared to Helios$^+$ Tregs found in the TdLN (Figure **2G,H**). TNFR2, PD-1 and OX40 expression were not further increased. Additionally, tumor-resident Helios$^+$ Tregs uniquely expressed CXCR6 and CD39. Although present in a significantly smaller proportion (Figure **1I**), we observed that tumor-resident Helios$^-$ Tregs displayed a comparable phenotype to tumor-resident Helios$^+$ Tregs (Figure **S1C-E**). Taken together, these findings suggest that TC-1 tumor growth preferentially drives effector differentiation of Helios$^+$ Tregs in the TdLN, which likely enables their subsequent infiltration from the bloodstream into the tumor. In the tumor, the effector Treg phenotype is most explicitly present.

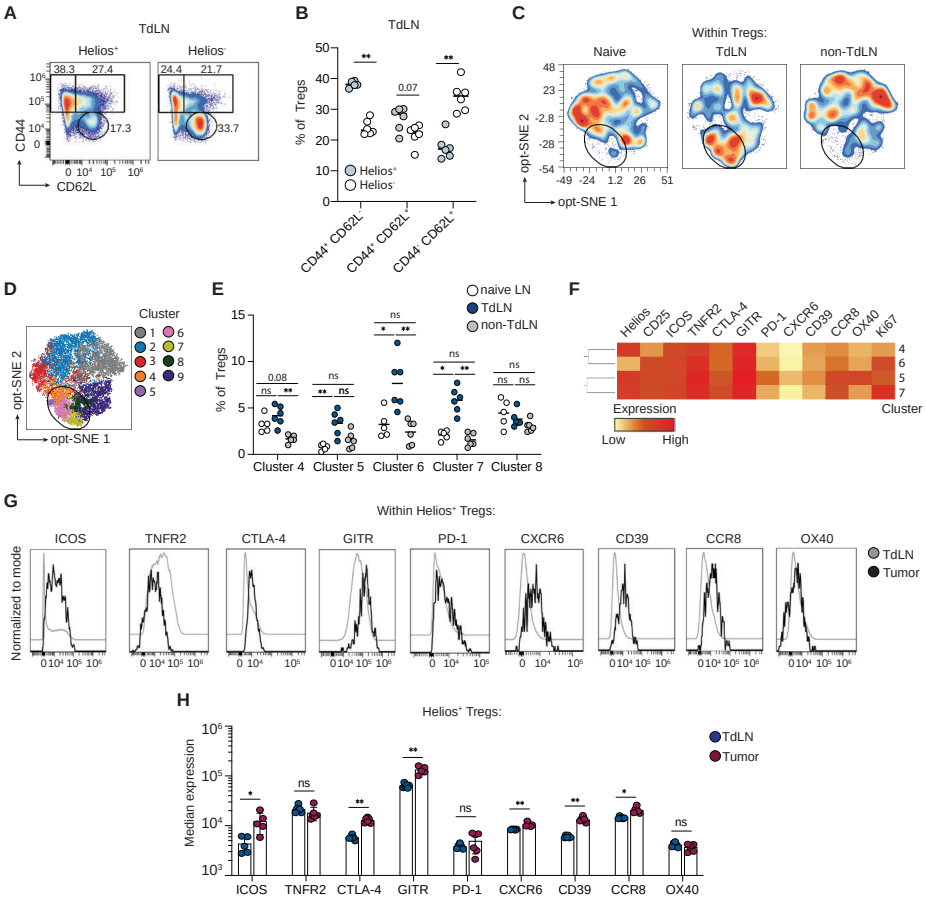

Figure 2. Helios⁺ Tregs acquire a more explicit effector phenotype in the TME.
Phenotypic analysis by flow cytometry of the Treg population found in the TdLN (right axillary LN), non-TdLN (left inguinal LN) and tumor of mice bearing 50 mm² TC-1 tumors (n=6) or age-matched naïve mice (n=5). (**A,B**) Representative concatenated (n=6) flow cytometry plots (**A**) and quantification (**B**) of the percentage of Helios⁺ and Helios⁻ Tregs expressing CD44 and/or CD62L. The numbers in (A) represent percentages. (**C**) Opt-SNE display of 1000 randomly selected Treg cells per sample found in axillary LNs of naïve mice (n=5), together with TdLN and non-TdLN of TC-1 tumor bearing mice (n=6). Black circle is for visualization purposes only. (**D**) Opt-SNE visualization of 9 Treg clusters identified by FlowSOM. Black circle visualizes the clusters with upregulated activation markers, as indicated in Figure **S1B**. (**E**) Quantification of the indicated clusters identified in (D) in naïve LNs, TdLNs and non-TdLNs. (**F**) Heatmap overview of the relative expression of the indicated Treg markers among clusters 4, 5, 6 and 7. (**G,H**) Representative (n = 5-6) concatenated histograms (**G**) and quantification (**H**) depicting expression of the indicated markers on Helios⁺ Tregs found in the TdLN and tumor. Results are combined from two separate experiments.
Error bars indicate SD. *P < 0.05, **P < 0.01, Mann-Whitney test in (B) and (H). Kruskal-Wallis with Dunn's post hoc test in (E). ns; no significance.

Discussion

Tregs are among the first immune cells to respond to tumor development[24], establishing an immunosuppressive environment that could hinder anti-tumor immune responses[3,31]. These Tregs tend to accumulate in the TdLN before migrating into the tumor[24]. However, the precise mechanisms governing tumor-induced Treg priming in the TdLN and their subsequent migration into the tumor remain poorly understood. Recent studies found significant overlap in TCR sequences between Tregs isolated from the tumor and blood, but not with Tconv cells[5,14,32]. This suggest peripheral Treg recruitment and potential activation upon recognition of antigens distinct from those recognized by Tconvs[33,34]. Additionally, tumor-associated Tregs likely resemble tissue-resident Tregs[5,15,35], complicating targeted intervention without affecting healthy tissue Tregs.

To identify potential therapeutic targets, we need to better understand the mechanisms underlying tumor-induced Treg priming and the subsequent migration and adaptation of these Tregs in the TME. Hence, we require effective *in vivo* tumor models that can recapitulate this process. Our study demonstrates that the TC-1 tumor model is suitable for this purpose. Specifically, we identify that tumor development favors expansion of Helios$^+$ Tregs, representing tTregs, in the TdLN. These Tregs then migrate into the tumor where they further adopt a matured phenotype. To gain a better understanding of the observed findings, future experiments should focus on the underlying mechanisms governing Treg priming in the tumor setting. For instance, scRNAseq, together with TCR sequencing of Tregs extracted from the TdLN and tumor, compared to healthy LN and lung tissue (considering TC-1 tumors originate from lung epithelial cells[25]), may identify specific cellular states and pathways distinguishing normal tissue-resident from tumor-specific Tregs. This data may be particularly important to gain insights into the differentiation trajectories of Tregs in the TdLN. Additionally, this data will also provide a better understanding of the overlap between tumor-infiltrating Tregs and those residing in healthy tissue. Particularly, it has been described that Tregs transitioning from the TdLN into the tumor undergo an adaptation process to become tumor-resident Tregs[30]. However, it remains unclear whether these findings resemble a common tissue-resident adaptation process[15,36], or if they are exclusive to the tumor context. This could potentially be addressed by scRNAseq data from our setting. Finally, given the proportion of Helios$^-$ Tregs present in the TdLN, CD4$^+$ Tconv cells should be analyzed in parallel. By performing TCR sequencing analysis, it could be determine whether these cells are pTregs originating from Tconv conversion within the TdLN[37].

An alternative approach worth exploring involves scRNAseq together with multiplex spectral flow cytometry to analyze the immune composition in the TdLN and compare it to healthy LNs. Specifically, it would be interesting to map the myeloid population, including dendritic cells (DCs) and monocytes to identify cellular states that may dictate Treg priming[38]. By utilizing the fluorescent protein zsGreen, stably transduced in TC-1 tumor cells, sorting strategies could efficiently identify recently migrated DCs and other myeloid populations from the tumor[39]. This

information may help to identify how tumor development impacts DC and myeloid functional states, potentially favoring Treg differentiation over Tconv priming.

Studies in humans have demonstrated that tumor-resident Tregs acquire an enhanced immunosuppressive phenotype compared to Tregs derived from healthy tissue[16,40]. This suggests the existence of additional contributing factors that may sustain the intra-tumoral Treg pool and impact their molecular reprogramming, such as local interactions with DCs[21,41] or macrophages[42]. Considering that TC-1 tumors primarily contain myeloid populations, it would be interesting to better understand the interplay between these cells with tumor-resident Tregs. Immunohistochemistry (IHC) on entire slide images may help to determine the spatial localization of Tregs and DCs or macrophages in the tumor. In addition, intervention studies including CSF1R-targeted depletion[43,44] or CCR2-inhibitors[45,46] are required to determine the interaction between macrophages and Tregs. While these interventions may offer clarity regarding the general interplay between these cell types, further exploration into the phenotypic and functional changes occurring in these cells subsequent to these interventions is essential. Particularly, it would be intriguing to dissect the mechanisms employed by myeloid cells that contribute to Treg differentiation within the TME. This can either be through direct interactions with potential co-inhibitory or -stimulatory receptors[47], or through indirect mechanisms like the release of cytokines[45,47]. The collective insights from this data could potentially provide a strategy to alleviate immunosuppression within the TME, not by targeting Tregs directly, but by focusing on modulating tumor-resident myeloid cells.

Taken together, we here show that the TC-1 tumor model may be used to delineate the mechanisms guiding tumor-induced Treg differentiation in TdLN and the tumor. Furthermore, we suggest potential avenues for investigating Treg differentiation mechanisms in the tumor context. These efforts are vital for identifying potential therapeutic targets.

Methods

Murine TC-1 tumor cell line

The TC-1 tumor cell line is derived from C57BL/6 lung epithelial cells engineered to express HPV16 E6 and E7 proteins[25] and was received from Leiden University Medical Center in 2015. TC-1 cells were cultured in RPMI 1640 (Gibco, Life Technologies), supplemented with 10% fetal calf serum (FCS), 0.1 mM non-essential amino acids, 1 mM sodium pyruvate, 2 mM L-glutamine, 10 mM HEPES and penicillin/streptomycin (Roche) at 37°C, 5% CO_2 and the stock was tested negative for *Mycoplasma* by PCR. Thawed cells were used within 3 passages for *in vivo* experiments.

Mice

Six-to-eight-week old female C57BL/6jRj mice were obtained from Janvier Laboratories (le Genest Saint Isle, France) and maintained in individually ventilated cages (Innovive) under specific pathogen-free conditions. All mouse experiments were performed in accordance with institutional and national guidelines and were approved by the Animal Welfare Body (IVD) of the Netherlands Cancer Institute.

Tumor transplantation

Mice were anesthetized with isofluorane and injected subcutaneously (s.c.) with $1x10^5$ TC-1 tumor cells in 50 µl HBSS. Tumor size was measured by calipers in two dimensions and calculated as: area (mm^2) = width x length. Mice were sacrificed at the indicated timepoints, when humane endpoint was reached or when the tumor size reached >100 mm^2.

FTY720 treatment

When tumor size reached 18-20 mm^2 (day 0), TC-1 tumor bearing mice were treated with the sphingosine-1-phosphate receptor-1 agonist FTY720 (Fingolimod, Cayman Chemical), dissolved in 0.9% NaCl solution (vehicle) and administered at 2 mg/kg by oral gavage. FTY720 treatment was repeated at day 4 and 6 and mice were sacrificed at day 9.

Tissue preparation and flow cytometry

Lymphoid tissues and tumors were harvested from mice at the indicate timepoints. To characterize the TdLN and non-TdLNs, we performed intra-tumoral injection of 5% Evans Blue Dye (Sigma-Aldrich) in 50 µl PBS under isofluorane, and identified the axillary lymph node as the TdLN, whereas the contralateral inguinal LN was defined as the non-TdLN. Tumor tissue was mechanically disaggregated using a McIlwain tissue chopper (Mickle Laboratory Engineering), and a single-cell

suspension was prepared by digesting the tissue in collagenase type A (Roche) and 25 µg/ml DNase I (Sigma) in serum-free DMEM for 45 min at 37°C. Enzyme activity was neutralized by addition of medium containing 10% FCS, and the tissue was dispersed by passing through a 70-µm cell strainer. To acquire single cell suspensions of LNs and spleen, the tissue was punctured with a 27 G needle followed by incubation in 100 µg/mL LiberaseTM TL (Roche) in serum-free DMEM for 30 min at 37°C. Enzyme activity was neutralized as described above and tissue was dispersed by passing through a 70-µm cell strainer. For surface staining, single cells of the isolated tissues were first incubated with anti-CD16/32 (1:50, clone 2.4G2, BD Bioscience) supplemented with 10 µg/ml DNAse, to block unspecific Fc receptor binding, for 10 min on ice. Next, surface antibody staining was performed (Table 1) for 30 min in PBS containing 0.5% BSA and 0.01% sodium azide. For intracellular staining of transcription factors and cytokines, cells were fixed and permeabilized with the FOXP3 Transcription Factor Staining Buffer Set according to the manufacturer's protocol (Thermo Fischer Scientific). Dead cells were excluded by using Fixable Viability Near-infra red dye (1:1000, Life Technologies) or Zombie UV fixable viability Kit (1:500, BioLegend). Absolute cell numbers were determined by adding AccuCount Blank Particles (7-7.9 µm, Spherotech) to each sample, prior to flow cytometry analysis. Fluorescence minus one (FMO) was used as a negative control for activation markers. Flow cytometry was performed using a BD FACSymphonyTM A5 SORP flow cytometer or the 5-laser Cytek Aurora. All generated data was analyzed using OMIQ software (Dotmatics, Boston, MA).

Data analysis

Dimensionality reduction and FlowSOM[48] analysis of flow cytometry data was performed using OMIQ software. Following conventional marker expression analysis, the population of interest was manually gated, and down-sampling was performed to select the maximal number of cells per tissue representative for all tissue types included, as indicated in the figure legends. K-means clustering of the indicated populations was performed using FlowSOM, including all markers indicated, except for live/dead, CD45, CD3 and CD4. Dimension reduction and visualization was performed using uniform manifold approximation and projection (UMAP) analysis[49], including the same markers as described above and by using the default OMIQ settings.

Statistical analysis

All statistical data were analyzed using GraphPad Prism version 9 (GraphPad Software, La Jolla, CA). Statistical analyses were performed as indicated in the figure legends. A P value < 0.05 was considered statistically significant; *$p<0.05$, **$p<0.01$, ***$p<0.001$, ****$p<0.0001$. Data are represented as mean + S.D.

References

1 Vignali, D. A., Collison, L. W. & Workman, C. J. How regulatory T cells work. *Nat Rev Immunol* **8**, 523-532 (2008).

2 Shang, B., Liu, Y., Jiang, S. J. & Liu, Y. Prognostic value of tumor-infiltrating FoxP3+ regulatory T cells in cancers: a systematic review and meta-analysis. *Sci Rep* **5**, 15179 (2015).

3 Kumagai, S. *et al.* The PD-1 expression balance between effector and regulatory T cells predicts the clinical efficacy of PD-1 blockade therapies. *Nat Immunol* **21**, 1346-1358 (2020).

4 Wing, J. B., Tanaka, A. & Sakaguchi, S. Human FOXP3(+) Regulatory T Cell Heterogeneity and Function in Autoimmunity and Cancer. *Immunity* **50**, 302-316 (2019).

5 Delacher, M. *et al.* Single-cell chromatin accessibility landscape identifies tissue repair program in human regulatory T cells. *Immunity* **54**, 702-720 e717 (2021).

6 Josefowicz, S. Z. *et al.* Extrathymically generated regulatory T cells control mucosal TH2 inflammation. *Nature* **482**, 395-399 (2012).

7 Samstein, R. M., Josefowicz, S. Z., Arvey, A., Treuting, P. M. & Rudensky, A. Y. Extrathymic generation of regulatory T cells in placental mammals mitigates maternal-fetal conflict. *Cell* **150**, 29-38 (2012).

8 Liston, A. & Gray, D. H. Homeostatic control of regulatory T cell diversity. *Nat Rev Immunol* **14**, 154-165 (2014).

9 Josefowicz, S. Z., Lu, L. F. & Rudensky, A. Y. Regulatory T cells: mechanisms of differentiation and function. *Annu Rev Immunol* **30**, 531-564 (2012).

10 Koenen, H. J. *et al.* Human CD25highFoxp3pos regulatory T cells differentiate into IL-17-producing cells. *Blood* **112**, 2340-2352 (2008).

11 Opstelten, R. *et al.* GPA33: A Marker to Identify Stable Human Regulatory T Cells. *J Immunol* **204**, 3139-3148 (2020).

12 Yates, K., Bi, K., Haining, W. N., Cantor, H. & Kim, H. J. Comparative transcriptome analysis reveals distinct genetic modules associated with Helios expression in intratumoral regulatory T cells. *Proc Natl Acad Sci U S A* **115**, 2162-2167 (2018).

13 Nakagawa, H. *et al.* Instability of Helios-deficient Tregs is associated with conversion to a T-effector phenotype and enhanced antitumor immunity. *Proc Natl Acad Sci U S A* **113**, 6248-6253 (2016).

14 Ahmadzadeh, M. *et al.* Tumor-infiltrating human CD4(+) regulatory T cells display a distinct TCR repertoire and exhibit tumor and neoantigen reactivity. *Sci Immunol* **4** (2019).

15 Miragaia, R. J. *et al.* Single-Cell Transcriptomics of Regulatory T Cells Reveals Trajectories of Tissue Adaptation. *Immunity* **50**, 493-504 e497 (2019).

16 Plitas, G. *et al.* Regulatory T Cells Exhibit Distinct Features in Human Breast Cancer. *Immunity* **45**, 1122-1134 (2016).

17 Nunez, N. G. *et al.* Tumor invasion in draining lymph nodes is associated with Treg accumulation in breast cancer patients. *Nat Commun* **11**, 3272 (2020).

18 Kos, K. *et al.* Tumor-educated T(regs) drive organ-specific metastasis in breast cancer by impairing NK cells in the lymph node niche. *Cell Rep* **38**, 110447 (2022).

19 Reticker-Flynn, N. E. *et al.* Lymph node colonization induces tumor-immune tolerance to promote distant metastasis. *Cell* **185**, 1924-1942 e1923 (2022).

20 Zagorulya, M. *et al.* Tissue-specific abundance of interferon-gamma drives regulatory T cells to restrain DC1-mediated priming of cytotoxic T cells against lung cancer. *Immunity* **56**, 386-405 e310 (2023).

21 Bauer, C. A. *et al.* Dynamic Treg interactions with intratumoral APCs promote local CTL dysfunction. *J Clin Invest* **124**, 2425-2440 (2014).

22 Salmon, H. *et al.* Expansion and Activation of CD103(+) Dendritic Cell Progenitors at the Tumor Site Enhances Tumor Responses to Therapeutic PD-L1 and BRAF Inhibition. *Immunity* **44**, 924-938 (2016).

23 Broz, M. L. *et al.* Dissecting the tumor myeloid compartment reveals rare activating antigen-presenting cells critical for T cell immunity. *Cancer Cell* **26**, 638-652 (2014).

24 Darrasse-Jeze, G. *et al.* Tumor emergence is sensed by self-specific CD44hi memory Tregs that create a dominant tolerogenic environment for tumors in mice. *J Clin Invest* **119**, 2648-2662 (2009).

25 Lin, K. Y. *et al.* Treatment of established tumors with a novel vaccine that enhances major histocompatibility class II presentation of tumor antigen. *Cancer Res* **56**, 21-26 (1996).

26 Thorsson, V. *et al.* The Immune Landscape of Cancer. *Immunity* **48**, 812-830 e814 (2018).

27 Frijlink, E. *et al.* (2023).

28 Matloubian, M. *et al.* Lymphocyte egress from thymus and peripheral lymphoid organs is dependent on S1P receptor 1. *Nature* **427**, 355-360 (2004).

29 Thornton, A. M. *et al.* Expression of Helios, an Ikaros transcription factor family member, differentiates thymic-derived from peripherally induced Foxp3+ T regulatory cells. *J Immunol* **184**, 3433-3441 (2010).

30 Li, Z. *et al.* In vivo labeling reveals continuous trafficking of TCF-1+ T cells between tumor and lymphoid tissue. *J Exp Med* **219** (2022).

31 Deng, L. *et al.* Accumulation of foxp3+ T regulatory cells in draining lymph nodes correlates with disease progression and immune suppression in colorectal cancer patients. *Clin Cancer Res* **16**, 4105-4112 (2010).

32 Wang, L. *et al.* Connecting blood and intratumoral T(reg) cell activity in predicting future relapse in breast cancer. *Nat Immunol* **20**, 1220-1230 (2019).

33 Hindley, J. P. *et al.* Analysis of the T-cell receptor repertoires of tumor-infiltrating conventional and regulatory T cells reveals no evidence for conversion in carcinogen-induced tumors. *Cancer Res* **71**, 736-746 (2011).

34 Sainz-Perez, A., Lim, A., Lemercier, B. & Leclerc, C. The T-cell receptor repertoire of tumor-infiltrating regulatory T lymphocytes is skewed toward public sequences. *Cancer Res* **72**, 3557-3569 (2012).

35 Malchow, S. *et al.* Aire-dependent thymic development of tumor-associated regulatory T cells. *Science* **339**, 1219-1224 (2013).

36 Li, C. *et al.* TCR Transgenic Mice Reveal Stepwise, Multi-site Acquisition of the Distinctive Fat-Treg Phenotype. *Cell* **174**, 285-299 e212 (2018).

37 Alonso, R. *et al.* Induction of anergic or regulatory tumor-specific CD4(+) T cells in the tumor-draining lymph node. *Nat Commun* **9**, 2113 (2018).

38 Maldonado, R. A. & von Andrian, U. H. How tolerogenic dendritic cells induce regulatory T cells. *Adv Immunol* **108**, 111-165 (2010).

39 Binnewies, M. *et al.* Unleashing Type-2 Dendritic Cells to Drive Protective Antitumor CD4(+) T Cell Immunity. *Cell* **177**, 556-571 e516 (2019).

40 De Simone, M. *et al.* Transcriptional Landscape of Human Tissue Lymphocytes Unveils Uniqueness of Tumor-Infiltrating T Regulatory Cells. *Immunity* **45**, 1135-1147 (2016).

41 Marangoni, F. *et al.* Expansion of tumor-associated Treg cells upon disruption of a CTLA-4-dependent feedback loop. *Cell* **184**, 3998-4015 e3919 (2021).

42 Casanova-Acebes, M. *et al.* Tissue-resident macrophages provide a pro-tumorigenic niche to early NSCLC cells. *Nature* **595**, 578-584 (2021).

43 Kos, K. *et al.* Tumor-associated macrophages promote intratumoral conversion of conventional CD4(+) T cells into regulatory T cells via PD-1 signalling. *Oncoimmunology* **11**, 2063225 (2022).

44 Gyori, D. *et al.* Compensation between CSF1R+ macrophages and Foxp3+ Treg cells drives resistance to tumor immunotherapy. *JCI Insight* **3** (2018).

45 Mondini, M. *et al.* CCR2-Dependent Recruitment of Tregs and Monocytes Following Radiotherapy Is Associated with TNFalpha-Mediated Resistance. *Cancer Immunol Res* **7**, 376-387 (2019).

46 Liang, H. *et al.* Host STING-dependent MDSC mobilization drives extrinsic radiation resistance. *Nat Commun* **8**, 1736 (2017).

47 Lindau, D., Gielen, P., Kroesen, M., Wesseling, P. & Adema, G. J. The immunosuppressive tumour network: myeloid-derived suppressor cells, regulatory T cells and natural killer T cells. *Immunology* **138**, 105-115 (2013).

48 Van Gassen, S. *et al.* FlowSOM: Using self-organizing maps for visualization and interpretation of cytometry data. *Cytometry A* **87**, 636-645 (2015).

49 Becht, E. *et al.* Dimensionality reduction for visualizing single-cell data using UMAP. *Nat Biotechnol* **37**, 38-44 (2018).

Supplementary Data

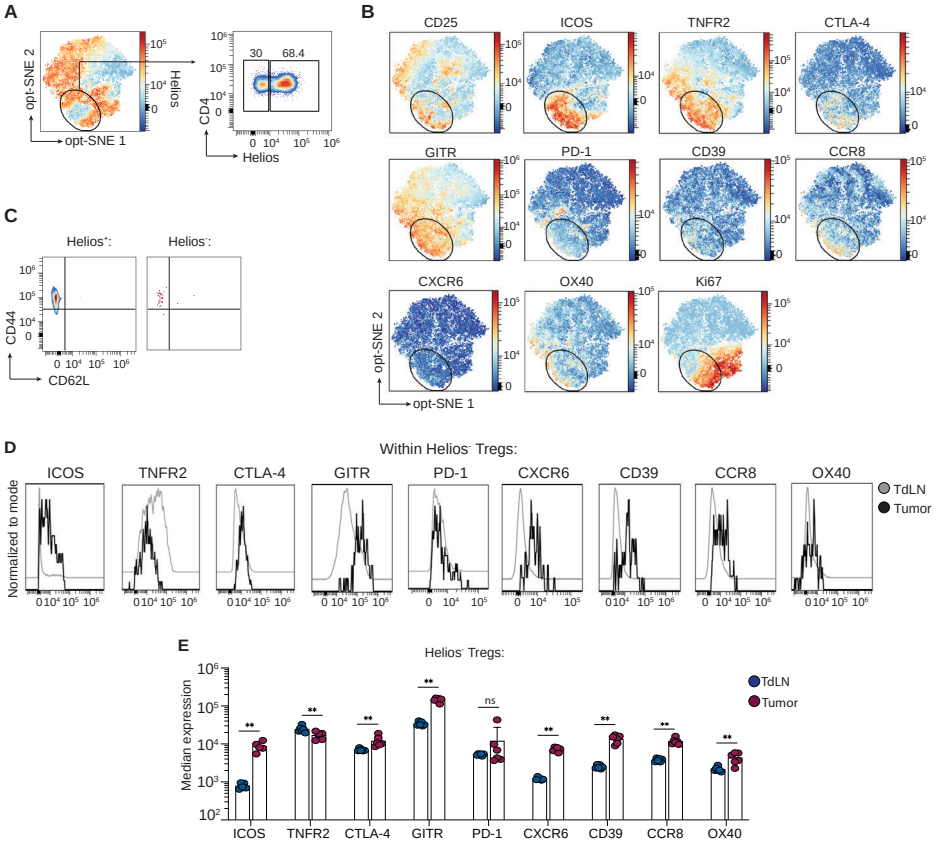

Supplemental Figure 1 – Related to Figure 2.
Phenotypic analysis by flow cytometry of the Treg population found in the TdLN, non-TdLN and tumor of mice bearing 50 mm^2 TC-1 tumors (n=6) or age-matched naïve mice (n=5). (**A,B**) Opt-SNE visualization of 1000 randomly selected Tregs per sample found in axillary LNs of naïve mice (n = 5), together with TdLN and non-TdLN of TC-1 tumor bearing mice (n=6). (**A**) Heatmap display (left) and representative flow plots (right) showing Helios expression. The figure on the right shows Helios expression as found among clusters 4-8 (see Figure **2D**). The numbers indicate percentages. (**B**) Representative heatmap visualization of the markers used to identify different activation states among Tregs. (**C**) Representative concatenated (n=6) flow cytometry plots of the proportion of tumor-derived $Helios^+$ and $Helios^-$ Tregs expressing CD44 and/or CD62L. (**D,E**) Representative concatenated (n=6) histograms (**D**) and quantification (**E**) depicting expression of the indicated markers on $Helios^-$ Tregs found in the TdLN and tumor. Error bars indicate SD. **P < 0.01, Mann-Whitney test in (E). ns; no significance.

Table 1: Antibodies & Reagents

Flow Cytometry Antibodies				
→ Antigen	*Fluorochrome*	*Clone*	*Vendor*	*Catalog #*
CD25	BV421	7D4	BD Biosciences	564571
CD3	PerCP eF710	500A2	eBiosciences	46-0033-82
CD3	BV785	17A2	BioLegend	100232
CD4	BUV395	GK1.5	BD Biosciences	563790
CD45	APC/Fire810	30-F11	BioLegend	103173
CD45	BUV563	30-F11	BD Biosciences	612924
CD8	BB515	53-6.7	BD Biosciences	564422
CD8	BUV805	53-6.7	BD Biosciences	612898
CTLA-4	BV605	UC10-4B9	BioLegend	106323
FOXP3	APC	FJK-16S	eBiosciences	25-5773-82
FOXP3	PE Cy5.5	FJK-16S	eBiosciences	35-5773-80
Helios	PE Cy7	22F6	BioLegend	137235
ICOS	PerCP Cy5.5	C398.4A	BioLegend	313518
CD39	BUV805	24DMS1	eBiosciences	368-0391-82
TNFR2	PE	TR75-89	BioLegend	113405
Ki67	AF700	SolA15	eBiosciences	56-5698-82
Ki67	eFluor506	SolA15	eBiosciences	69-5698-80
CXCR6	APC/Cy7	SA051D1	BioLegend	151124
GITR	R718	DTA-1	BD Optibuild	2285946
OX40	SB780	OX-86	eBiosciences	78-1341-82
CCR8	BV711	SA214G2	BioLegend	150320
PD-1	BUV737	J43	eBiosciences	376-9985-80
CD44	BV785	IM7	BioLegend	103059
CD62L	APC/Cy7	MEL-14	BD Biosciences	560514

Viability dyes		
LIVE/DEAD™ Fixable Near-IR Dead Cell Stain Kit	Thermo Fisher	L10119
Zombie UV™ Fixable Viability Kit	Biolegend	423107

In vivo antibodies & reagents				
Antigen	Immunogen	Clone	Vendor	Catalog #
FTY720			Cayman Chemical Company	10006292